http://journal.uir.ac.id/index.php/JGEET

E-ISSN: 2541-5794
P-ISSN: 2503-216X

Journal of Geoscience,
Engineering, Environment, and Technology
Vol 8 No 1 2023

RESEARCH ARTICLE

Electrical Resistance Tomographic by Using Current Injection and Magnetic Field Induction

Dudi Darmawan[1]*, Deddy Kurniadi[2], Suprijanto[2]

[1] *Engineering Physics, Universitas Telkom, Jl Telekomunikasi no 1, Jawa Barat, Indonesia*
[2] *Instrmentasi dan Kontrol, Institut Teknologi Bandung, Jl. Ganesha 10, Jawa Barat, Indonesia*

* Corresponding author: dudiddw@telkomuniversity.ac.id
Tel.:+081320500247
Received: Sep 20, 2022; Accepted: Mar 17, 2023.
DOI: 10.25299/jgeet.2023.8.1.10560

Abstract

A critical issue in electrical tomography is ill-posed problems due to low sensitivity. In the electric current injection method, the placement of the injection electrode on the object boundary can influence it. This condition causes the reconstruction result of parameter change far away from the boundary to be inferior in quality. Another excitation method is using magnetic field induction proposed to overcome these problems. Each reconstruction image was obtained using two methods with three types of parameter changes, that represented the edge and the center of the object position. Both reconstruction results are merged and further processed to enhance the quality of the image, based on the average value of the resistivity of each element. The results show that the final image reconstruction has a smaller root mean square error (RMSE) than the electric current injection method.

Keywords: Ill-posed; sensitivity; current injection; magnetic field induction; reconstruction image

1. Introduction

An important issue in electrical impedance tomography is ill-posed problems (Gong *et al.*, 2016) (López C. *et al.*, 2015) (Harikumar, Prabu, and Raghavan, 2013) (Khan and Ling, 2019). The things that cause the appearance of ill-posed are mismatch model, non-linear, low sensitivity, and the limited amount of data (information) (Alsaker, Hamilton, and Hauptmann, 2017) (Seppänen *et al.*, 2009) (Chitturi and Farrukh, 2017). These factors have been the subject of attention from some of the research related to current injection tomography.

The issue of sensitivity is influenced by several factors, including the large injection currents, the current position of the injection point, the position of the measurement electrodes, and electrode measurement conditions. These factors form a system of data collection on the current injection tomography. Therefore, a solution to overcome this problem is to find the appropriate configuration of data collection systems, such as adjacent, cross, opposite, multi-reference, and adaptive. However, all of those data collection systems use excitation electrodes attached to the object boundaries. This condition causes the changes in the parameters in the middle of the object to be hard to be detected.

Another method that can be used to overcome the low sensitivity is the use of another excitation method, i.e. the magnetic field. The induction of a magnetic field to the inside of the object is expected to overcome the low sensitivity. This is possible because the stimulation of the magnetic field is done to the entire object (Wang *et al.*, 2018) (Feldkamp and Quirk, 2019) (Ma, Wei, and Soleimani, 2013) (Ma and Soleimani, 2017). In this way, the same sensitivity to the whole object can be reached so that the spatial resolution of the uniform resistivity distribution is obtained (Seppänen *et al.*, 2009) (Chitturi and Farrukh, 2017).

However, this raises another problem which is irregularities of the magnetic field given part. The solution to solve this issue is to find the optimal configuration of the induction system (Darmawan *et al.*, 2015) (Wang *et al.*, 2018) (Alsaker, Hamilton, and Hauptmann, 2017). The induction system includes the shape and dimensions of the coil inducer, induction number, position, and configuration of the induction. One form of alternative coil used is the rectangular coil that has been used for imaging using the eddy current method (Deddy Kurniadi, 2014) (Darmawan *et al.*, 2015). Experiments were performed using a variety of frequency values and give good results. Therefore, the selection of a rectangular shape is attractive to apply to the case of tomography. This form is believed to provide the homogeneous distribution of the magnetic field, especially attached to the square-shaped object.

Therefore, the incorporation of the current injection method for magnetic field induction method is attractive for development. The ability of the current injection method in detecting parameter changes in the edge can be accomplished by the method of magnetic field induction. Providing a magnetic field to the center of the object is expected to address the issue of sensitivity in the current injection method.

This study was conducted to obtain the reconstructed image of each method. Furthermore, both image reconstruction results are combined and evaluated. This image fusion has been widely used in various image processing and merging methods (Rane, Kakde, and Jain, 2017) (Zhao, Li, and Cheng, 1993).

2. Methods

2.1 Forward and Inverse Model of Current Injection Method

In the current injection method, an electrical current is injected through some point in the object's surface. Currents will spread and cause electric potential distribution inside the object. The relationship between the electric potential (V), and resistivity (r) was formulated by the Laplace equation (Darmawan *et al.*, 2016) (Ma and Soleimani, 2017) (Darbas *et al.*, 2021).

$$\nabla \cdot \frac{1}{\rho}\nabla V = 0 \quad \text{in } \Omega \tag{1}$$

With boundary conditions of potential and current density on the surface,

$$V = V_0 \qquad \text{on } \partial\Omega \tag{2}$$

$$\frac{1}{\rho}\frac{\partial V}{\partial n} = J_0 \text{ on } \partial\Omega \tag{3}$$

In the current injection tomography, the forward model is the mapping function that states the value of the electric potential distribution as a function of the resistivity distribution, $F(\rho) \rightarrow \boldsymbol{V}|_{\Omega}\_\Omega$. The electric potential function is obtained through the solution of the Laplace equation.

In this study, a solution of forward models is obtained through the concept of current conservation. This concept states that the net amount of current in each element is equal to zero. In other words, the current coming into each element is equal to the current coming out of that element.

In the case of two dimensions, the concept of current conservation is obtained through the application of double integrals in equation (1).

$$\iint_S \left(\nabla \cdot \frac{1}{\rho}\nabla V\right) \cdot dS = 0 \tag{4}$$

By using the divergence theorem, the surface integral along S on the left side of equation (4) turns into an integral along a closed path l surrounding one element.

$$\oint_l \frac{1}{\rho}\nabla \boldsymbol{V} \cdot dl = 0 \tag{5}$$

The left side of equation (5) states the sum of the current flux penetrated to the entire surface of the boundary surrounding the element.

In 2 dimensions, numerical solutions to equation (5) produce equation (6).

$$\sum_l \frac{1}{\rho}\nabla \boldsymbol{V} \,.\, \Delta l = 0 \tag{6}$$

with the boundary condition being current flux density (Je, i) [15].

$$J_{e(i)} = \begin{cases} J, for\ \ injected\ element \\ 0, for\ not\ injected\ element \end{cases}$$

This is a Neumann boundary condition.

Furthermore, equation (6) is applied to all elements and produces some linear equations connecting the potential value of an element with the potential values of neighboring elements. The linear equations of potential values of all elements can be arranged in the matrix-vector form, such as equation (7).

$$G_{N\times N}.\ \bar{V}_{N\times 1} = \bar{C}_{N\times 1} \tag{7}$$

with

G = admittance matric
$\bar{V}$ = potential vector
$\bar{C}$ = current source vector
N = number of elements

Furthermore, obtaining the resistivity distribution from the boundary potential distribution observed is done by using the linearization method. A function that maps the boundary potential distribution back into the resistivity distribution, $F^{-1}[V] \rightarrow \sigma|_{\Omega}$ is known as the inverse model. Through the linearization method, it was found that changes in resistivity become proportional to the potential boundary changes, according to the equation (8).

$$\Delta\bar{V} = S\,\Delta\bar{\rho} \tag{8}$$

with S as the sensitivity matrix.

The Tikhonov regularization (Dingley and Soleimani, 2021) is used to get a solution so that equation (8) turns into equation (9).

$$\Delta\bar{\rho} = (S + \alpha I)^{-1}\Delta\bar{V} \tag{9}$$

And finally, resistivity reconstruction results were obtained through

$$\rho_{anomali} = \rho_{homogen} + \Delta\bar{\rho} \tag{10}$$

Reconstruction results are evaluated numerically using the parameters of root mean square (RMS) as equation (11), and it's called Error.

$$Error = \frac{1}{N}\sqrt{\left(\rho_{rekonstruksi} - \rho_{uji}\right)^2} \tag{11}$$

2.2 Forward and Inverse Model of Magnetic Field Method

In the method of magnetic field induction, the magnetic field change is raised in the coil. The induced current will appear in the object. The relationship between the electric potential (V), resistivity (ρ), and magnetic potential (A) is defined by equation (12), which is known as Poisson's equation [20]

$$\nabla \cdot \frac{1}{\rho}\nabla V = -\omega A\,\nabla\frac{1}{\rho} \tag{12}$$

The solution of equation (12) is obtained by the same approach as in section 2.1.

$$\iint_S \left(\nabla \cdot \frac{1}{\rho}\nabla V\right) dS = \iint_S \left(-\boldsymbol{\omega A}\,\boldsymbol{\nabla}\frac{1}{\rho}\right) dS \tag{13}$$

The Numerical solution of equation (13) is equation (14).

$$\sum_l \frac{1}{\rho}\nabla \boldsymbol{V} \,.\, \Delta l = -\,\omega A \,.\, \nabla\frac{1}{\rho}\,\Delta S \tag{14}$$

Furthermore, the completion of some linear equations of all elements is done using equation (7).

2.3 Magnetic Field Simulation

Calculation of the magnetic field $\vec{A}$ by the rectangular coil is carried out as follows:

Induction of a magnetic field at a point by the $\overrightarrow{dl}$ conductive segment which is electrified by I satisfies the Biot-Savart equation.

$$\vec{A} = \int \frac{\mu_o I}{4\pi} \frac{\vec{dl}\, x\, \hat{r}}{r^2} \tag{15}$$

with

$\vec{A}$ = Magnetic field
μ_0 = permeability
I = current
$\vec{dl}$ = coil segment
r = distance to the observation point

If defined $r = \sqrt{x^2 + y^2 + z^2}$ and $K = \frac{\mu_0}{4\pi}$ then the magnitude of the magnetic field by the current conductive segment is formulated in equation (16).

$$\vec{dA} = \frac{\mu_o I}{4\pi} \frac{\vec{dl} \times \hat{r}}{r} = KI \frac{\left(\hat{\imath}\, dx + \hat{\jmath}\, dy + \hat{k}\, dz\right)}{r} \times \frac{\vec{r}}{r} \tag{16}$$

The magnitude of the magnetic potential by the conductor along L is obtained by integrating equation (16) so that the magnetic potential is obtained by a straight conductor in equation (17).

$$\vec{A} = KI \int_0^L \frac{\left(\hat{\imath}\, dx + \hat{\jmath}\, dy + \hat{k}\, dz\right)}{r} \times \frac{\vec{r}}{r} \tag{17}$$

Thus the magnetic potential by the four sides of the rectangular coil conductor is obtained by adding up the magnetic field potential by the four rectangular sides.

$$\vec{A} = \sum_1^4 KI \int_0^L \frac{\left(\hat{\imath}\, dx + \hat{\jmath}\, dy + \hat{k}\, dz\right)}{r} \times \frac{\vec{r}}{r} \tag{18}$$

The following is a numerical calculation of the magnetic field potential by one side of the rectangular coil. Suppose the starting point of the line conductor is at coordinates (x1, y1) and the endpoint of the line conductor is at coordinates (x2, y2). Divide the length of the conduit into n-line segments. If the distance of the two points to the observation surface is the same, z1 = z2 = z.

The length of each delivery segment is

$$\Delta x = \frac{x_2 - x_1}{n}$$

$$\Delta y = \frac{y_2 - y_1}{n}$$

The distance of a certain conductive segment to the magnetic potential calculation point satisfies equation (19)

$$r^2 = \left(x_p - x_1\right)^2 + \left(y_p - y_1\right)^2 + \left(z_p - z_1\right)^2 \tag{19}$$

The magnetic potential components of any segment satisfy equation (20).

$$\Delta A_{xi} = \frac{KI\left(z_p - z\right)\Delta y}{r}$$

$$\Delta A_{yi} = \frac{-KI\left(z_p - z\right)\Delta x}{r}$$

$$\Delta A_{zi} = \frac{KI[(y_p - y)\Delta x - (x_p - x)\Delta y]}{r} \tag{20}$$

The magnetic potential component at an observation point by all conveying segments satisfies equation (21).

$$A_x = \sum_{i=1}^{n} \Delta A_{xi}, \quad A_y = \sum_{i=1}^{n} \Delta A_{yi} \quad , A_z = \sum_{i=1}^{n} \Delta A_{zi} \tag{21}$$

The magnitude of the resultant magnetic potential at a point is obtained by complying with equation (22).

$$A = \sqrt{{A_x}^2 + {A_y}^2 + {A_z}^2} \tag{22}$$

3. Results and Discussion

3.1 Simulation Results of Forward and Inverse Model of Current Injection Method

The simulation results of the forward model using the method of the adjacent, cross, and opposite injection with 16 times the injection shown in figure 1.

The simulation results for the best reconstruction of the current injection method with three different anomalies are shown in table 1.

The simulation of the forward model of magnetic field induction is done 16 times. Simulation results which show the distribution of magnetic field and electric potential distribution produced, are shown in figure 2.

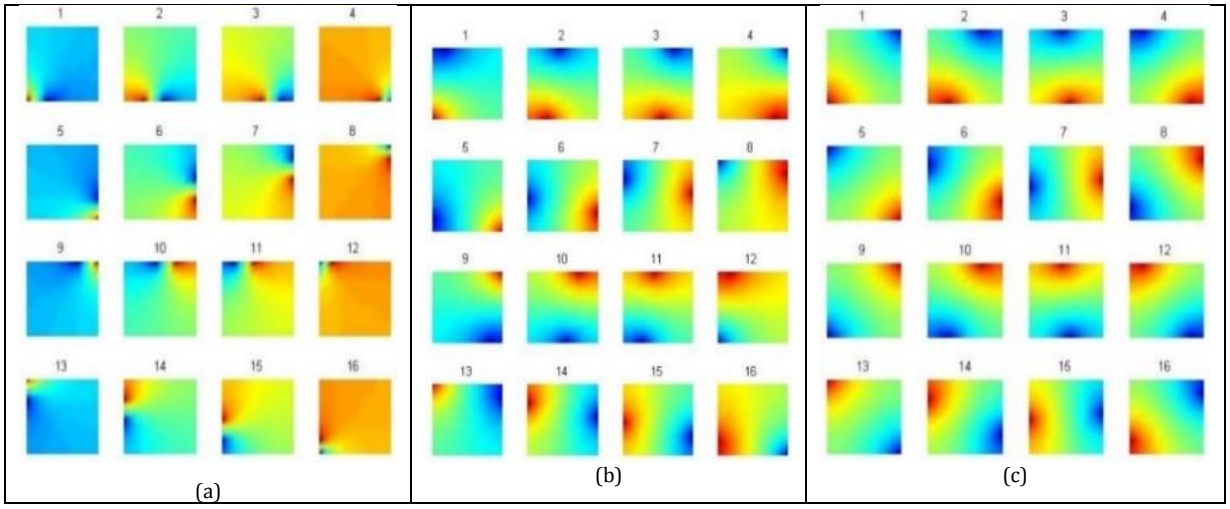

Fig. 1. Potential distribution as the solution of the forward model of current injection method (a) adjacent (b) cross (c) opposite.

3.2 Simulation Results of Forward and Inverse Model of Magnetic Field Induction Method

The simulation of the forward model of magnetic field induction is done 16 times. Simulation results show the distribution of magnetic field and electric potential distribution produced, shown in figure 2.

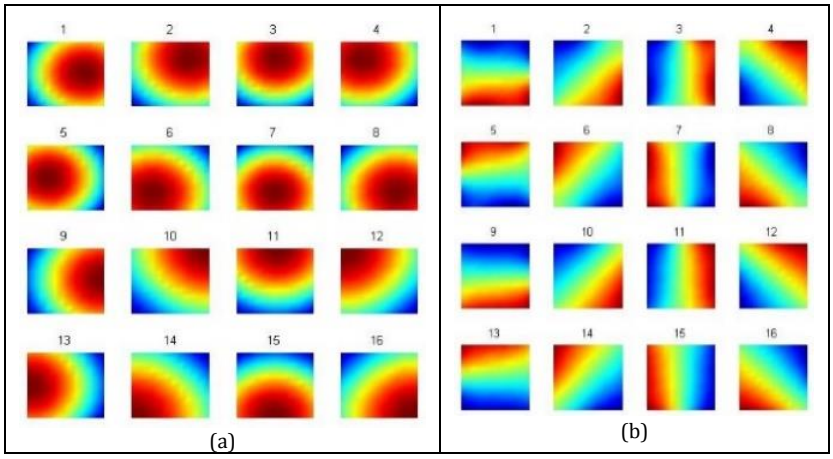

Fig. 2. (a) Magnetic field distribution and (b) Potential distribution as the forward model solution of magnetic field induction method.

Table 1. Reconstruction Results Of Resistivity Distribution By Current Injection Method

Anomaly	Reconstruction results in 16 times Induction Image	Error
		0,0071
		0,0102
		0,0086
Average		0,0086

Table 2. Reconstruction Results Of Resistivity Distribution By Magnetic Field Induction Method

Anomaly	Reconstruction results of 16 times Injection Image	Error
		0,0060
		0,0080
		0,0090
Average		0,0077

Furthermore, in the same way as the current injection method, determining the resistivity distribution on the magnetic field induction method is performed using equation (6) in equation (10). The best reconstruction results obtained are shown in table 2.

3.3 Merging of Reconstruction Result of Current Injection and Magnetic Field Induction

Merging cell value of the reconstruction results between the current injection and magnetic field method is conducted using 4 ways, namely minimum, maximum, max-min, and average value (Kumar *et al.*, 2016) (Arai, 2020) (Noushad, 2017) (Wang, 2020).

- Minimum value

This way takes the smallest value of the value of each element of both methods, thus formulated as

$$\rho = MIN\big(\rho(k), \rho(d)\big)$$

- Maximum value

This way takes the greatest value from the value of each element of both methods, thus formulated as

$$\rho = MAX\big(\rho(k), \rho(d)\big)$$

- Max-Min value

This way retrieves the value of the smallest value of both methods if both resistivity values are smaller than a specified value and takes the greatest value if both resistivity values are greater than that specified value.

$$\rho\_ = \begin{cases} MIN\big(\rho(k), \rho(d)\big), \rho(k) \;\; and \;\; \rho(d) < \delta \\ MAX\big(\rho(k), \rho(d)\big), \rho(k) \; and \; \rho(d) > \delta \\ AVG\big(\rho(k), \rho(d)\big), \;\; for \; others \end{cases}$$

- Average value

This way takes the value of the average of the value of both methods, thus formulated as

$$\rho = \big(\rho(k) + \rho(d)\big)/2$$

with

k index for injection

d index for induction

By using these ways, the simulation results of the merging of the two methods are shown in table 3.

4. Conclusion

The results of the reconstruction of the two methods, which were carried out separately, confirmed the advantages of each method. Tomography using the current injection method gives better results in detecting anomalies at the edges. While the magnetic field induction method gives better results in detecting anomalies in the middle of the test object.

Furthermore, merging the reconstructed image of the two methods increases in image quality. This is indicated by the merged image which is better than the reconstructed image of each method. Through the three types of anomalies tested, the average method produces better results.

Acknowledgments

This work is supported by Hibah Penelitian Pasca Doktor 2019, Ministry of Research, Technology and Higher Education of the Republic of Indonesia

References

Alsaker, M., Hamilton, S. J. and Hauptmann, A. (2017) 'A direct D-bar method for partial boundary data electrical impedance tomography with a priori information', *Inverse Problems and Imaging*, 11(3), pp. 427–454. doi: 10.3934/ipi.2017020.

Arai, K. (2020) 'Image restoration based on maximum entropy method with parameter estimation by means of annealing method', *International Journal of Advanced Computer Science and Applications*, 11(8), pp. 255–261. doi: 10.14569/IJACSA.2020.0110833.

Chitturi, V. and Farrukh, N. (2017) 'Spatial resolution in electrical impedance tomography: A topical review', *Journal of Electrical Bioimpedance*, 8(1), pp. 66–78. doi: 10.5617/jeb.3350.

Darbas, M. *et al.* (2021) 'Sensitivity analysis of the complete electrode model for electrical impedance tomography', *AIMS Mathematics*, 6(7), pp. 7333–7366. doi: 10.3934/math.2021431.

Darmawan, D. *et al.* (2015) 'Study of Induced Current Electrical Impedance Tomography Configuration on 2 Dimensional Rectangular Object', *Proceedings of the 2014 International Conference on Physics and its Applications*, 1(June 2016). doi: 10.2991/icopia-14.2015.12.

Darmawan, D. *et al.* (2016) 'Applied current injection and magnetic field induction simultaneously on electrical impedance tomography', *International Journal of Tomography and Simulation*, 29(1).

Deddy Kurniadi, J. (2014) 'Electrical Impedance Tomography in Rectangular Object Using Data Collection System Based on Absolute Boundary Potential Measurement', *Mycobacterial Diseases*, 04(02), pp. 2–6. doi: 10.4172/2167-7964.1000160.

Dingley, G. and Soleimani, M. (2021) 'Multi-frequency magnetic induction tomography system and algorithm for imaging metallic objects', *Sensors*, 21(11). doi: 10.3390/s21113671.

Feldkamp, J. R. and Quirk, S. (2019) 'Internal magnetic induction tomography using a single coil', *Progress in Electromagnetics Research*, 164(December 2018), pp. 97–107. doi: 10.2528/PIER18120408.

Gong, B. *et al.* (2016) 'EIT Image Reconstruction by Modified Data', *Journal of Biomedical Science and Engineering*, 09(10), pp. 99–106. doi: 10.4236/jbise.2016.910b013.

Harikumar, R., Prabu, R. and Raghavan, S. (2013) 'Electrical Impedance Tomography (EIT) and Its Medical Applications : A Review', *International Journal of Soft Computing and Engineering (IJSCE)*, 3(4), pp. 193–198. Available at: http://scholar.google.com/scholar?hl=en&btnG=Search&q=intitle:Electrical+Impedance+Tomography+(+EIT+)+and+Its+Medical+Applications+:+A+Review#0.

Khan, T. A. and Ling, S. H. (2019) 'Review on electrical impedance tomography: Artificial intelligence methods and its applications', *Algorithms*, 12(5). doi: 10.3390/a12050088.

Kumar, K. *et al.* (2016) 'Content Based Image Retrieval Using Gray Scale Weighted Average Method', *International Journal of Advanced Computer Science and Applications*, 7(1), pp. 1–6. doi: 10.14569/ijacsa.2016.070101.

López C., D. C. *et al.* (2015) 'Nonlinear ill-posed problem analysis in model-based parameter estimation and experimental design', *Computers and Chemical Engineering*, 77, pp. 24–42. doi: 10.1016/j.compchemeng.2015.03.002.

Ma, L. and Soleimani, M. (2017) 'Magnetic induction tomography methods and applications: A review', *Measurement Science and Technology*, 28(7). doi: 10.1088/1361-6501/aa7107.

Ma, L., Wei, H. Y. and Soleimani, M. (2013) 'Planar magnetic induction tomography for 3D near subsurface imaging', *Progress in Electromagnetics Research*, 138(March), pp. 65–82. doi: 10.2528/PIER12110711.

Noushad, M. (2017) 'Image Pair Fusion using Weighted Average Method', 3(10), pp. 397–402.

Rane, N. D., Kakde, P. B. and Jain, P. M. (2017) 'Comparative study of Image Fusion Methods : A Review', *International Journal of Engineering and Applied Sciences*, 4(10), pp. 67–72.

Seppänen, A. *et al.* (2009) 'Electrical resistance tomography imaging of concrete', *Concrete Repair, Rehabilitation and Retrofitting II - Proceedings of the 2nd International Conference on Concrete Repair, Rehabilitation and Retrofitting, ICCRRR*, pp. 231–232. doi: 10.1201/9781439828403.ch79.

Wang, J. *et al.* (2018) 'Magnetic Induction Tomography Simulation Analysis Based on Comsol Multiphysics Soft', *IOP Conference Series: Materials Science and Engineering*, 394(4). doi: 10.1088/1757-899X/394/4/042001.

Wang, Y. (2020) 'Image segmentation method with maximum entropy optimized by Wolf pack algorithm', *Journal of Physics: Conference Series*, 1650(3). doi: 10.1088/1742-6596/1650/3/032042.

Zhao, Z., Li, X. and Cheng, H. D. (1993) 'Image enhancement using fuzzy logic', *International Conference on Fuzzy Theory and Technology Proceedings, Abstracts and Summaries*, pp. 74–75.